

Laboratory evidence for proton energization by collisionless shock surfing

W. Yao,^{1,2} A. Fazzini,¹ S. N. Chen,³ K. Burdonov,^{1,2} P. Antici,⁴ J. Béard,⁵ S. Bolaños,¹ A. Ciardi,² R. Diab,¹ E.D. Filippov,^{6,7} S. Kisyo,³ V. Lelasseux,¹ M. Miceli,⁸ Q. Moreno,^{9,10} V. Nastasa,³ S. Orlando,⁸ S. Pikuz,^{6,11} D. C. Popescu,³ G. Revet,¹ X. Ribeyre,⁹ E. d’Humières,⁹ and J. Fuchs¹

¹*LULI - CNRS, CEA, UPMC Univ Paris 06 : Sorbonne Université, Ecole Polytechnique, Institut Polytechnique de Paris - F-91128 Palaiseau cedex, France*

²*Sorbonne Université, Observatoire de Paris, Université PSL, CNRS, LERMA, F-75005, Paris, France*

³*ELI-NP, "Horia Hulubei" National Institute for Physics and Nuclear Engineering, 30 Reactorului Street, RO-077125, Bucharest-Magurele, Romania*

⁴*INRS-EMT, 1650 boul. Lionel-Boulet, Varennes, QC, J3X 1S2, Canada*

⁵*LNCMI, UPR 3228, CNRS-UGA-UPS-INSA, Toulouse 31400, France*

⁶*JiHT, Russian Academy of Sciences, 125412, Moscow, Russia*

⁷*IAP, Russian Academy of Sciences, 603155, Nizhny Novgorod, Russia*

⁸*INAF-Osservatorio Astronomico di Palermo, Palermo, Italy*

⁹*University of Bordeaux, Centre Lasers Intenses et Applications, CNRS, CEA, UMR 5107, F-33405 Talence, France*

¹⁰*ELI-Beamlines, Institute of Physics, Czech Academy of Sciences, 5 Kvetna 835, 25241 Dolni Brezany, Czech Republic*

¹¹*NRNU MEPhI, 115409, Moscow, Russia*

(Dated: 15 April 2022)

The origin of the high-energy particles flying through the Universe is still an open question¹. One identified source is collisionless shock waves formed when energy release from stars encounters the tenuous magnetized space environment^{2,3}. By interacting with the ambient, these shocks can transfer energy to particles, accelerating them^{4,5}. Characterization of these shocks has become very rich with satellite measurements at the Earth’s bow shock and powerful numerical simulations, however identifying the exact mechanism, or combination of mechanisms enabling particle acceleration is still widely debated^{1,3,6,7}. Here we show that astrophysically relevant super-critical quasi-perpendicular magnetized collisionless shocks can be produced and characterized in the laboratory. Moreover, we observe a “foot” in the shock profile that is characteristic of super-critical shocks as well as the energization of protons picked up from the ambient gas to hundred keV. Our kinetic particle-in-cell simulations modeling of our laboratory event identified shock surfing^{8,9} as the proton acceleration mechanism. Our observations not only provide the first direct evidence of early stage ion energization by collisionless shocks, but they also highlight the role this particular mechanism plays in energizing ambient ions to feed further stages of acceleration¹⁰. Furthermore, our results also open the door to future laboratory experiments investigating the possible transition to other mechanisms, when increasing the magnetic field strength, or the effect induced shock front ripples^{11,12} could have on acceleration processes.

The acceleration of energetic charged particles by collisionless shock waves is an ubiquitous phenomenon in

astrophysical environments, e.g. during the expansion of supernova remnants (SNRs) in the interstellar medium (ISM)¹³, during solar wind interaction with the Earth’s magnetosphere¹⁴, or with the ISM (at the so-called termination shock)¹⁵. Except for SNRs, where latest studies suggest that the acceleration is efficient at quasi-parallel shocks¹⁶, in the other cases, the shocks belong to the super-critical, high Mach-number, and quasi-perpendicular (i.e. the magnetic field is perpendicular to the shock propagation direction). These so-called super-critical shocks have a specific characteristic such that in addition to dissipation by thermalisation and entropy, energy is dissipated also by reflecting the upstream plasma. The threshold for this regime is set by a high Alfvénic Mach number $M_A = v_{sh}/v_A \gtrsim 2.7$ (where v_{sh} and v_A are the shock and Alfvénic velocity, respectively)⁶.

Three basic ion acceleration mechanisms are commonly considered to be induced by such shocks^{3,4,6}: diffusive shock acceleration (DSA), shock surfing acceleration (SSA), and shock drift acceleration (SDA). The first proceeds through multiple diffusion of particles on electromagnetic turbulence associated with the shock, while in SSA and SDA, the particles gyro-rotate (Larmor motion) in close proximity with the shock and gain energy through the induced electric field associated with the shock.

These last two processes are mostly differentiated by how and where the particles are trapped around the shock front and the ratio of the ion Larmor radius vs. the shock width (large for SSA and small for SDA)^{9,11}.

DSA, which is commonly invoked for high-energy particle acceleration in SNRs, is thought to require quite energetic particles to be effective^{8,17}, which raises the so-called “injection problem” of their generation¹⁸. Providing those pre-accelerated seed particles is precisely thought to be accomplished by SSA or SDA, which are

evoked to accelerate particle at low energies, e.g. in our solar system¹⁹.

Due to the small sampling of such phenomena even close to Earth, the complexity of the structuring of such shocks^{8,20}, and the related difficulty in modelling them realistically, the question of the effectiveness and relative importance of SDA and SSA¹¹ is still largely debated in the literature.

We will first show that laboratory experiments can be performed to generate and characterize globally mildly super-critical, quasi-perpendicular magnetized collisionless shocks. The shock shown in Fig. 1 is typically produced by using a laser-driven piston to send an expanding plasma into an ambient (a cloud of hydrogen) secondary plasma²¹ in an externally controlled magnetic field (see Methods). The high-strength applied magnetic field²² we use is key in order to ensure the collisionless nature of the induced shock. The key parameters of the laboratory created shock are summarized in Table 1, which shows that they compare favorably with the parameters of the Earth’s bow shock¹⁵, the solar wind termination shock^{23,24}, and typical non-relativistic SNR interactions with dense molecular clouds²⁵.

	M_A	$\lambda_{mfp}/r_{L,i}$
Our experiment	3.4	1.1×10^2
Bow Shock	3.0	1.2×10^8
Term. Shock	5.1	7.4×10^7
Mixed-morphology SNR	~ 6	$\geq 2.0 \times 10^2$

Table 1. Parameters of the laboratory shocks as well as that of three shocks found in natural events. The listed parameters for each plasma are: the Alfvénic Mach number (M_A , see text), and the ratio of the collisional mean free path (λ_{mfp}) over the ion Larmor radius ($r_{L,i}$). The first shows that all shocks are super-critical, the second shows that all shocks are collisionless, i.e. electromagnetic forces dominate over collisions since the collision mean free path is always much smaller than the ion Larmor radius. The three natural events are: the Earth’s bow shock, the solar wind termination shock, and low-velocity interactions of mixed-morphology SNRs with dense molecular clouds. Details on the parameters and how they are derived are given in Extended Data Table 1.

A snapshot of the integrated plasma electron density, obtained by optical probing at 4 ns after the laser irradiation of the target, is shown in Fig. 1c and d in the two perpendicular planes containing the main expansion axis. The laser comes from the right side and the piston source target is located at the left (at $x = 0$). We can clearly see both the piston front and the shock front (indicated by the orange and green arrows, respectively). A lineout of the plasma density is shown in Fig. 1e, where the piston and shock fronts are well identified by the abrupt density changes. The piston front is steepened by the compression induced by the magnetic field²⁶ (see also Extended Data Fig. 2). In contrast, when the B-field is switched off, only a smooth plasma expansion into the ambient

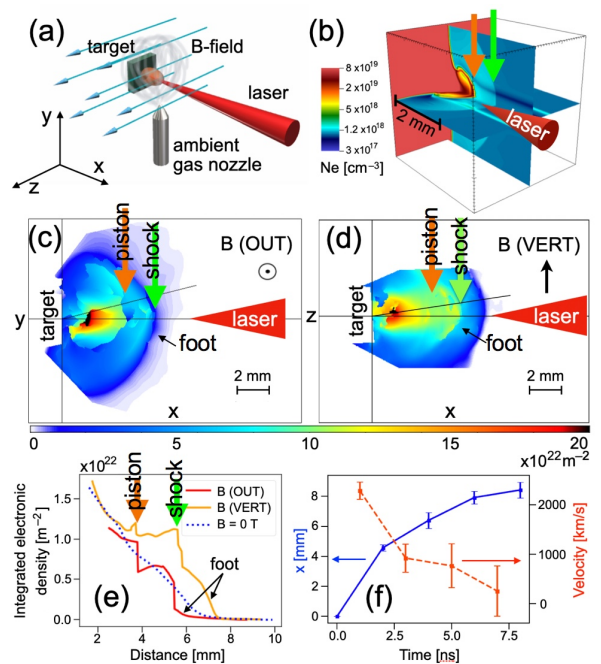


Figure 1. Configuration and characterization of the laboratory super-critical shock. (a) Cartoon of the setup of the experiment performed at JLF/Titan to characterize the shock. (b) Three-dimensional (3D) rendering of the ablated piston interacting with the magnetized ambient gas at 4 ns from the FLASH simulation (see Methods). The orange arrow represents the piston front, while the green one the shock front. (c) and (d) Experimental density measurement (integrated along the line of sight) 4 ns after the laser irradiation of the solid target (at $t = 0$) recorded in the two different and complementary xy and xz planes in order to characterize in three-dimensions the overall plasma. Each image corresponds to a different laser shot. More images at different times are shown in Extended Data Fig. 1. (e) Lineouts obtained from the images above, showing the integrated density along the black solid lines starting from the targets. (f) Evolution of the shock front position along the x -axis, and the corresponding velocity. Each point corresponds to the average of the shock front of all relevant shots. The error bars on the x position represent not only the maximum extent of the variation of the shock front position as observed in relevant shots, but they also integrate the uncertainty of the initial target surface ($x = 0$) as well as the width of the shock front. The error bars on the velocity correspond to the propagation of the errors on the position. The small relative error attests to the reproducibility of the overall experimental phenomenon.

(blue dashed line) can be seen. In the case when the magnetic field is applied, another clear signature of the magnetized shock, observed by satellite²⁷, is the noticeable feature of a “foot” in the density profile, located in the shock upstream (US). It is due to the cyclic evolution of the plasma: the plasma in the foot is picked up to form the shock front, while the latter is also periodically dismantled by the Larmor. The observed foot width is of the order 0.5-1 mm, which compares favourably with the expected foot width being twice the ion inertial length²⁸

(which is here $\approx 0.23\text{mm}$), and with the width observed in our simulations shown below.

Fig. 1f shows the shock front position evolution and the corresponding velocity deduced from it, which shows the very fast decrease of the shock velocity over the first few ns. Before 2.6 ns, the shock front velocity is around 1500 km/s, corresponding to an ion-ion collisional mean-free-path $\lambda_{mfp} \approx 10$ mm and the ion collisional time is $\tau_i \approx 6$ ns – both are larger than the interaction scale, indicating that the shock is collisionless. However, after 4-5 ns, the shock velocity decreases rapidly to about 500 km/s, thus becoming sub-critical and the foot of the shock becomes less distinguishable (see also in Extended Data Fig. 1).

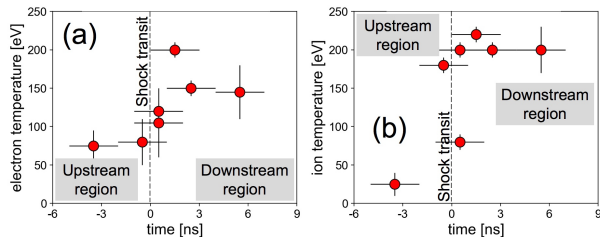


Figure 2. Laboratory characterization of electron and ion temperature increase in the shock. The measurements are performed at LULI2000, using collective Thomson scattering (TS) on the electron and ion waves in the plasma, in a fixed volume 4.3 mm away from the solid target surface, and with $B = 20$ T applied (see Methods). Time 0, at which a jump is identified, here corresponds to the time at which the shock is sweeping through the location of the measurement. Each data point corresponds to a shot. Panel (a) illustrates the local electron temperature inferred from both the measurements on the electron and ion waves. Panel (b) corresponds to the local ion temperature inferred from the measurement on the ion waves. The vertical error bars reflect the variations of the parameters when fitting the data with a theoretical fit, while still fitting well the data (see examples in Extended Data Fig. 3 and 4). The horizontal bar reflects the duration (3 ns) of the laser beam used to perform the measurement.

The plasma temperature was measured at a fixed location at different instants in time (see Methods), allowing to characterize the temperature increase in the shock as it swept through the probed volume, as shown in Fig. 2. Before the shock front, the electron and ion temperatures are of the order of a few tens of eV, and T_e is usually larger than T_i . While behind the shock front, the electron temperature is almost doubled (see Fig. 2a), the ion temperature is increased dramatically to about 200 eV, and T_i becomes larger than T_e . All of the above results are typical signs of a shock wave. Again, the formation of the shock is only possible due to the applied external magnetic field. In its absence, as shown in Extended Data Fig. 3, we witness no ion temperature increase in the same region. Extended Data Fig. 4 shows the electron density increase in the shock compared to that of the ambient.

Another important aspect of our experiment is the ob-

servation of non-thermal protons when the piston interacts with the magnetized ambient gas. The recorded spectra, shown in Fig. 3 (red dots), clearly show the presence of particle energization when the external magnetic field is applied. The cutoff energy reaches to about 0.08 MeV. We stress that without the external B-field or in the absence of ambient gas, no signal is recorded in the ion spectrometer (hidden under the experimental noise baseline, as indicated by the cyan dashed line in Fig. 3).

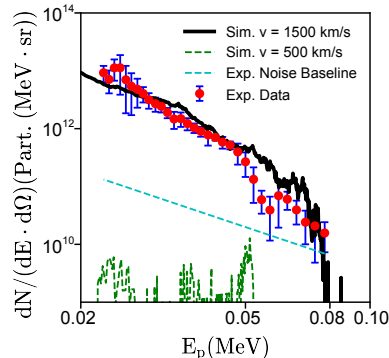


Figure 3. Evidence for the energization of protons picked up from the ambient. Proton energy spectra of both the experiment (red dots, averaged over five shots, as measured at LULI2000) and of two PIC simulations (black solid line for the high-velocity case with $v = 1500$ km/s and green dashed line for the low-velocity one with $v = 500$ km/s, both are measured at $t = 2.6$ ns in the simulations). The blue error bars correspond to one sigma deviation from the average (shown by the red dots), the noise level on the diagnostic is materialized by the cyan dashed line. Note that the absolute scale in proton numbers applies only to the experimental spectrum; the simulated spectrum is arbitrarily scaled to the experiment one.

Fig. 1b shows the result of a 3D magneto-hydrodynamic (MHD) simulation (performed using the FLASH code, see Methods) of the experiment. We observe that it reproduces globally the macroscopic expansion of the piston in the magnetized ambient gas and the shock formation (see also Extended Data Fig. 5). However, no foot can be observed. What is more, in the MHD simulation, the shock velocity is quite steady and does not show the strong and fast energy damping experienced by the shock from the experiment. Both facts point to a non-hydrodynamic origin of the foot and of the energy loss experienced by the shock in its initial phase. This is why, in the following, we resort to kinetic simulations with a Particle-In-Cell (PIC) code (the fully kinetic code SMILEI, see Methods). As the shock changes from super- to sub-critical in its evolution, we have performed simulations in two cases (see Fig. 3), i.e. with two different velocities representative of the two phases, i.e. 1500 and 500 km/s respectively to unveil the micro-physics responsible for the observed non-thermal proton acceleration.

The initial conditions of our large-scale PIC simula-

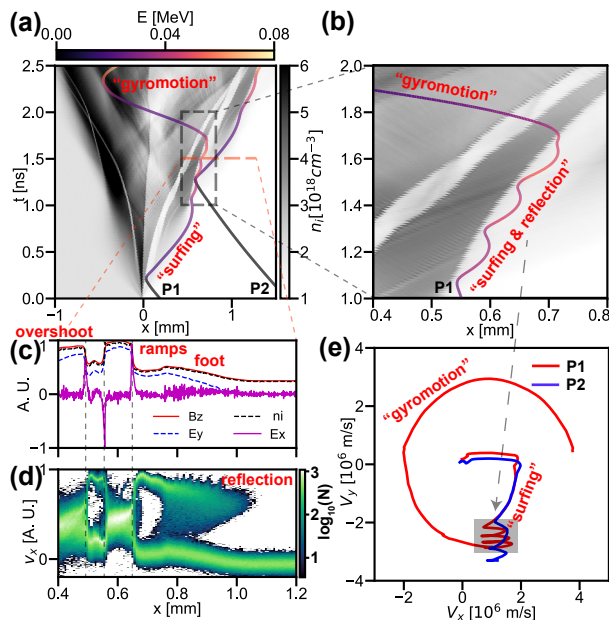


Figure 4. Dynamics of a high-velocity shock and of the subsequent shock surfing proton energization as analyzed by PIC simulations. (a) Trajectories of two representative protons (P1 and P2), energized from the ambient gas to > 0.06 MeV at $t=2.6$ ns in $x-t$ diagram, overlaid on the proton density map in the shock reference frame (having velocity 1500 km/s in the laboratory frame). (b) Zoom of the black dashed rectangle region in (a), showing the “surfing & reflection” of P1 along the forward shock. (c) Lineout of normalized density and electromagnetic fields at the red dashed line in (a) ($t = 1.5$ ns, $0.4 < x < 1.2$ mm). (d) The corresponding proton $x-v_x$ phase space diagram where the colorbar represents the normalized particle number N in logarithm scale. (e) The v_x-v_y diagram of P1 and P2. The grey shaded area corresponds to the “surfing & reflection” stage in (b).

tions use the experimentally characterized plasma conditions. Note that in order to directly compare with the experimental spectra, the ion specie in our simulation is proton with its real mass ($m_p/m_e = 1836$). The PIC simulation results, for the high-velocity case, are summarized in Fig. 4, which identifies clearly the underlying proton acceleration mechanism, matching the laboratory proton spectrum, to be SSA²⁹.

Fig. 4a illustrates the overall evolution of the early stage of the high-velocity shock. Shown is the proton density in the shock reference frame, where we can clearly see the density pileups in the forward direction, indicating the shock formation (and periodic reformation⁶). To elucidate the proton acceleration mechanism, a random sample of protons picked from the ambient, which will constitute the high-energy end of the spectrum shown in Fig. 3 (i.e. having energies > 0.06 MeV), are followed in the simulation. The trajectories of two representative ones (P1 and P2) are plotted in Fig. 4a. Following these trajectories, we can see that they are first picked up

by the forward shock at the shock front, and then they gain energy while “surfing” along (or confined around) the shock front. Besides, while surfing along the shock front, P1 gets trapped and reflected repeatedly, with a small energy perturbation, as is shown in Fig. 4b, all of which is typical of SSA.

Typical structures of the super-critical quasi-perpendicular collisionless shock⁶ can be also seen in Fig. 4c where we plot the lineout of density and electromagnetic (EM) fields around the shock front ($0.4 < x < 1.2$ mm in the shock reference frame), when the shock is fully formed ($t = 1.5$ ns).

The longitudinal electric field (E_x) is seen to peak right at the ramp, providing the electrostatic cross-shock potential to trap and reflect the protons (with a velocity lower than that of the shock). In the corresponding $x-v_x$ phase space in Fig. 4d, we can clearly see that, indeed, it is at the position of E_x that protons get reflected (see also Extended Data Fig. 6 for more time frames of this phase space, as well as for those corresponding to the simulation performed at low-velocity). This rules out the possibility of SDA, where the ion reflection is caused by the downstream compressed B-field¹⁷, being dominant. At last, as shown in Fig. 4e, the main contribution of the proton energy gain is due to v_y via the inductive electric field $E_y = v_x B_z$, which is again in accordance with the SSA mechanism³⁰.

The proton spectrum at $t = 2.6$ ns produced by the PIC simulated high-velocity shock, and which is shown in Fig. 3 (black solid line), is in remarkable agreement with the experimental observation. As in the experiment, no proton energization is found in the simulations performed without magnetic field or ambient medium. We note also that for the low-velocity shock (with $v = 500$ km/s), the spectrum (green dashed line) is far below the experimental noise baseline, indicating that the protons are indeed accelerated at the first 2–3 ns, when the shock is in the super-critical regime.

Hence, a remarkable outcome of our analysis is that, at the early stage of the shock formation and development, SSA can be considered as the sole mechanism in picking up thermal ions and accelerating them to hundred keV-scale energies. SSA appears to produce sufficiently energetic protons for further acceleration by DSA, as for example at the Earth’s bow shock, where the threshold energy for DSA to become effective is in the range of $\sim (50 - 100)$ keV/nucleon⁶. Since we are limited in time in exploring the dynamics of the protons interacting with the super-critical shock, we can only speculate that SDA might appear at a later stage, when the reflected ions acquire enough energy to cross the shock front.

We also note that usually detailed considerations of shock rippling and structuration are evoked in a possible competition between SSA and SDA in the solar wind^{11,12}, but that these were not required here in our analysis where we simulate an idealized flat shock front. Although we know that in the experiment, there is likely small structuring developing at the shock front (induced

by instabilities²⁶, but too small at this early stage to be resolved by our optical probing), these are obviously not required in the modelling to reproduce the experimentally observed energization.

Aside from the solar wind, another interesting case of a shock similar to that investigated here is that of supernova remnants (SNRs) interacting with dense molecular clouds, e.g. the class of Mixed-Morphology SNRs²⁵. A large fraction of these SNRs show indications of low energy (MeV) cosmic rays (CRs) interacting with the cloud material and ionising it^{31–33}. These mildly relativistic particles are typically explained as CRs accelerated in the past at the SNR shock front that escaped the remnant and reached the cloud³⁴. However, our results show that in-situ generation of CRs of low energy (\sim MeV) could be at play, and should be also taken into account³¹. The in-situ acceleration would be most likely generated by the low-velocity, mildly super-critical (see Table 1) SNR shock interacting with the dense cloud; a scenario which is supported by our findings.

In conclusion, our experiment provides strong evidence for the generation of super-critical quasi-perpendicular magnetized collisionless shocks in the laboratory. More importantly, non-thermal proton spectra are observed; in our kinetic simulations, they are recognized to be produced by SSA alone.

The platform we used can be tuned in the future to monitor the transition to DSA, which should be favored by varying the magnetic field orientation, using even higher-strength magnetic field³⁵ or higher-velocity jets driven by short-pulse lasers as pistons³⁶. Another direction will be to test quantitatively the effect of intentionally rippling the shock front by seeding the piston plasma with modulations³⁷.

Acknowledgments The authors would like to thank the teams of the LULI (France) and JLF laser (USA) facilities for their expert support, as well the Dresden High Magnetic Field Laboratory at Helmholtz-Zentrum Dresden-Rossendorf for the development of the pulsed power generator used at LULI. We thank the Smilei dev-team for technical support. We also thank Ph. Savoini (Sorbonne U., France), L. Gremillet and C. Ruyer (CEA-France) for discussions. W.Y. would like to thank R. Li (SZTU, China) for discussions. This work was supported by funding from the European Research Council (ERC) under the European Unions Horizon 2020 research and innovation program (Grant Agreement No. 787539). Part of the experimental system is covered by a patent (1000183285, 2013, INPI-France). The FLASH software used was developed, in part, by the DOE NNSA ASC and the DOE Office of Science ASCR-supported Flash Center for Computational Science at the University of Chicago. The research leading to these results is supported by Extreme Light Infrastructure Nuclear Physics (ELI-NP) Phase II, a project co-financed by the Romanian Government and European Union through the European Regional Development Fund. JIHT RAS team

members are supported by grant No. 13.1902.21.0035 in the form of a subsidy from the Ministry of Science and Higher Education of the Russian Federation. The reported study was funded by the Russian Foundation for Basic Research, project No. 19-32-60008.

Author contributions

J.F. and S.N.C. conceived the project. A.F., S.N.C., K.B., J.B., S.B., S.K., V.L., V.N., S.P., D.C.P., G.R. and J.F. performed the experiments. A.F., E.D.F., S.N.C., K.B., R.D., S.P. and J.F. analyzed the data. X.R. performed and analyzed the FLASH simulations, while W.Y. and A.F. performed and analyzed the SMILEI simulations, both with discussions with P.A., A.C., Q.M., X.R., E.d.H. and J.F. W.Y., S.N.C., and J.F. wrote the bulk of the paper, with major contributions from K.B., M.M. and S.O. All authors commented and revised the paper.

Competing interests The authors declare no competing interests.

Materials and correspondence Correspondence and material requests should be addressed to julien.fuchs@polytechnique.edu

Data availability All data needed to evaluate the conclusions in the paper are present in the paper. Experimental data and simulations are respectively archived on servers at LULI and LERMA laboratories and are available from the corresponding author upon reasonable request.

Code availability The code used to generate Fig. 1b is FLASH. The code used to generate part of Fig. 3 and Fig. 4 is SMILEI. Both codes are detailed in the Methods section.

- ¹Butt, Y. Beyond the myth of the supernova-remnant origin of cosmic rays. *Nature* **460**, 701–704 (2009).
- ²Sagdeev, R. Z. Cooperative phenomena and shock waves in collisionless plasmas. *Rev. Plasma Phys.* **4**, 23 (1966).
- ³Marcowith, A. *et al.* The microphysics of collisionless shock waves. *Reports on Progress in Physics* **79**, 046901 (2016).
- ⁴Blandford, R. & Eichler, D. Particle acceleration at astrophysical shocks: A theory of cosmic ray origin. *Physics Reports* **154**, 1–75 (1987).
- ⁵Aharonian, F. *et al.* High-energy particle acceleration in the shell of a supernova remnant. *Nature* **432**, 75–77 (2004).
- ⁶Balogh, A. & Treumann, R. A. *Physics of collisionless shocks: space plasma shock waves* (Springer New York, New York, NY, 2013).
- ⁷Marcowith, A. *et al.* Multi-scale simulations of particle acceleration in astrophysical systems. *Living Reviews in Computational Astrophysics* **6**, 1–182 (2020).
- ⁸Lee, M. A., Shapiro, V. D. & Sagdeev, R. Z. Pickup ion energization by shock surfing. *Journal of Geophysical Research: Space Physics* **101**, 4777–4789 (1996).
- ⁹Shapiro, V. D. & Üçer, D. Shock surfing acceleration. *Planetary and Space Science* **51**, 665–680 (2003).
- ¹⁰Ackermann, M. *et al.* A cocoon of freshly accelerated cosmic rays detected by fermi in the cygnus superbubble. *Science* **334**, 1103–1107 (2011).

- ¹¹Yang, Z., Lembège, B. & Lu, Q. Impact of the rippling of a perpendicular shock front on ion dynamics. *Journal of Geophysical Research: Space Physics* **117** (2012).
- ¹²Chalov, S., Malama, Y., Alexashov, D. & Izmodenov, V. Acceleration of interstellar pickup protons at the heliospheric termination shock: Voyager 1/2 energetic proton fluxes in the inner heliosheath. *Monthly Notices of the Royal Astronomical Society* **455**, 431–437 (2016).
- ¹³Helder, E. A. *et al.* Measuring the Cosmic-Ray Acceleration Efficiency of a Supernova Remnant. *Science* **325**, 719 (2009).
- ¹⁴Turner, D. L. *et al.* Autogenous and efficient acceleration of energetic ions upstream of earth’s bow shock. *Nature* **561**, 206–210 (2018).
- ¹⁵Decker, R. *et al.* Mediation of the solar wind termination shock by non-thermal ions. *Nature* **454**, 67–70 (2008).
- ¹⁶Caprioli, D. & Spitkovsky, A. Simulations of Ion Acceleration at Non-relativistic Shocks. I. Acceleration Efficiency. *Astrophys. J.* **783**, 91 (2014).
- ¹⁷Zank, G., Pauls, H., Cairns, I. & Webb, G. Interstellar pickup ions and quasi-perpendicular shocks: Implications for the termination shock and interplanetary shocks. *Journal of Geophysical Research: Space Physics* **101**, 457–477 (1996).
- ¹⁸Lembège, B. *et al.* Selected problems in collisionless-shock physics. *Space Science Reviews* **110**, 161–226 (2004).
- ¹⁹Burrows, R., Zank, G., Webb, G., Burlaga, L. & Ness, N. Pickup ion dynamics at the heliospheric termination shock observed by voyager 2. *The Astrophysical Journal* **715**, 1109 (2010).
- ²⁰Caprioli, D., Pop, A.-R. & Spitkovsky, A. Simulations and Theory of Ion Injection at Non-relativistic Collisionless Shocks. *Astrophysical J. L.* **798**, L28 (2015).
- ²¹Schaeffer, D. B. *et al.* Direct observations of particle dynamics in magnetized collisionless shock precursors in laser-produced plasmas. *Physical Review Letters* **122**, 245001 (2019).
- ²²Albertazzi, B. *et al.* Production of large volume, strongly magnetized laser-produced plasmas by use of pulsed external magnetic fields. *Review of Scientific Instruments* **84**, 043505 (2013).
- ²³Richardson, J. D., Kasper, J. C., Wang, C., Belcher, J. W. & Lazarus, A. J. Cool heliosheath plasma and deceleration of the upstream solar wind at the termination shock. *Nature* **454**, 63–66 (2008).
- ²⁴Burlaga, L. *et al.* Magnetic fields at the solar wind termination shock. *Nature* **454**, 75–77 (2008).
- ²⁵Rho, J. & Petre, R. Mixed-morphology supernova remnants. *The Astrophysical Journal Letters* **503**, L167 (1998).
- ²⁶Khiar, B. *et al.* Laser-produced magnetic-rayleigh-taylor unstable plasma slabs in a 20 t magnetic field. *Physical Review Letters* **123**, 205001 (2019).
- ²⁷Giagkiozis, S., Walker, S. N., Pope, S. A. & Collinson, G. Validation of single spacecraft methods for collisionless shock velocity estimation. *Journal of Geophysical Research: Space Physics* **122**, 8632–8641 (2017).
- ²⁸Baraka, S. Large scale earth’s bow shock with northern imf as simulated by pic code in parallel with mhd model. *J. Astrophys. Astr.* **37**, 14 (2016).
- ²⁹Katsouleas, T. & Dawson, J. Unlimited electron acceleration in laser-driven plasma waves. *Physical Review Letters* **51**, 392 (1983).
- ³⁰Matsukiyo, S. & Scholer, M. Microstructure of the heliospheric termination shock: Full particle electrodynamic simulations. *Journal of Geophysical Research: Space Physics* **116** (2011).
- ³¹Nobukawa, K. K. *et al.* Neutral iron line in the supernova remnant ic 443 and implications for mev cosmic rays. *Publications of the Astronomical Society of Japan* **71**, 115 (2019).
- ³²Nava, L. *et al.* Non-linear diffusion of cosmic rays escaping from supernova remnants - II. Hot ionized media. *Monthly Notices of the Royal Astronomical Society* **484**, 2684–2691 (2019).
- ³³Okon, H., Imai, M., Tanaka, T., Uchida, H. & Tsuru, T. G. Probing cosmic rays with fe k- α line structures generated by multiple ionization process. *Publications of the Astronomical Society of Japan* **72**, L7 (2020).
- ³⁴Phan, V. H. M. *et al.* Constraining the cosmic ray spectrum in the vicinity of the supernova remnant w28: from sub-gev to multi-tev energies. *A&A* **635**, A40 (2020).
- ³⁵Fujioka, S. *et al.* Kilotesla magnetic field due to a capacitor-coil target driven by high power laser. *Scientific Reports* **3**, 1170 (2013).
- ³⁶Kar, S. *et al.* Plasma jets driven by ultraintense-laser interaction with thin foils. *Physical Review Letters* **100**, 225004 (2008).
- ³⁷Cole, A. J. *et al.* Measurement of rayleigh–taylor instability in a laser-accelerated target. *Nature* **229**, 329–331 (1982).